PHYSICAL REVIEW D **72,** 024018 (2005)

Double-domain spectral method for black hole excision data

Marcus Ansorg

Max-Planck-Institut für Gravitationsphysik, Albert Einstein Institut, Am Mühlenberg 1, D-14476 Golm, Germany

(Received 12 May 2005; published 22 July 2005)

In this paper a new double-domain spectral method to compute binary black hole excision initial data is presented. The method solves a system of elliptic partial differential equations in the exterior of two excised spheres. At the surface of these spheres, boundary conditions need to be imposed. As such, the method can be used to construct arbitrary initial data corresponding to binary black holes with specific boundary conditions at their apparent horizons. We give representative examples corresponding to initial data that fulfill the requirements of the quasistationary framework, which combines the thin-sandwich formulation of the constraint equations with the isolated horizon conditions for black holes in quasiequilibrium. For all examples considered, numerical solutions with extremely high accuracy were obtained with moderate computational effort. Moreover, the method proves to be applicable even when tending toward limiting cases such as large radius ratios for the black holes.

DOI: 10.1103/PhysRevD.72.024018 PACS numbers: 04.25.Dm, 04.20.Ex, 04.70.Bw, 95.30.Sf

I. INTRODUCTION

Spectral methods utilizing multiple spatial domains have been used by many authors in order to solve elliptic partial differential equations in general relativity, see e.g. [1–10]. In this paper we demonstrate the strength of these methods by applying them to the calculation of initial data corresponding to binary black hole systems.

In a '3 + 1'-splitting of space and time, Einstein's equations may be formulated as constraint and evolution equations. The constraints form elliptic equations on spacelike hypersurfaces, which must be fulfilled by any data set that describes some initial state of the binary system. In constructing data of this kind, two different approaches have been explored, (i) puncture methods [11–16] and (ii) excision techniques [3,4,9,10,17–22].

In the puncture methods, a special polelike structure of the singularity inside the black hole is assumed which can be taken into account by a specific ansatz for the initial data. Therefore the relevant space for the constraint equations is all of $\mathbb{R}^3$. In contrast, the excision techniques solve the constraints only in the exterior of two excised spheroids within which the singularities are located. At the surface of these spheroids, special boundary conditions need to be imposed, see e.g. [3,4,9,10,17,18,23–25]. A promising approach for providing physically realistic data that describe binary systems in quasistationary orbits is given by the combination of the conformal thin-sandwich formulation [26,27] (for a review see [28]) and the isolated horizon framework [10,25,29–32]. While the conformal thin-sandwich equations incorporate the concept of quasistationarity into the constraint equations, the isolated horizon framework describes specific boundary conditions valid at the apparent horizons of the black holes that ensure a quasiequilibrium state.

In this paper, a new numerical scheme is presented that calculates binary black hole excision data by means of a double-domain spectral method. The scheme is an alternative approach to the spectral techniques used in [3,4] and to those utilized in [9,10]. It works on two spatial subdomains and requires relatively small spectral expansion orders to render highly accurate solutions. The complexity of the numerical scheme is comparable to the one presented in [16] for a single-domain puncture method, therefore allowing the code to run on a single processor.

The central idea of the method is the introduction of two spatial domains, within which the initial data admit a rapidly converging spectral expansion. In order to achieve this it is essential for the data to be smooth within these subdomains. At first, bispherical coordinates [33,34] are introduced through which the entire exterior of the two excised balls becomes the image of a single rectangular box (see Sec. II). In particular, a compactification of spatial infinity is realized, which corresponds to a mere line on a side of the box. However, as illustrated in Sec. III for the Laplace equation, a solution to an elliptic equation is in general only C^0 at this line, which suggests the introduction of an additional mapping. This map folds the box along the line in question, see Sec. IV. As a result, for a two-dimensional cross section, we get a domain of pentangular shape, which we divide up into two quadrangular ones. Each one of the two quadrangular regions is mapped diffeomorphically onto a square. As explained in Sec. V, spectral expansions for all data entries are carried out within these cuboids, and the collection of constraint equations, boundary, asymptotic fall off, regularity and transition conditions (the latter ones to be imposed at the boundary between the two domains) yield a complete set of equations to determine all spectral coefficients. We obtain the solution by means of a Newton-Raphson method. For a three-dimensional code, only an iterative scheme for executing the linear step inside the Newton solver is computationally affordable. Together with a reformulation of the regularity conditions (to be enforced at the axis along which the black holes are aligned) a specific plane relaxation scheme has been implemented that results

in a convergent iterative procedure. In Sec. VI we present first examples satisfying the equations and boundary conditions following from the above quasiequilibrium framework. We obtain extremely high accuracy even in limiting cases such as very large radius ratios for the excised spheres. Since only relatively little spectral resolution is needed, the code is of low computational cost. This makes it especially useful for the detailed study of wide classes of initial data sets. In Sec. VII we discuss future applications of the scheme, which will include a detailed mathematical and physical investigation of various initial data sets and the use of these data for a dynamical evolution.

II. BISPHERICAL COORDINATES

In this section we consider bispherical coordinates [33,34] through which the entire space exterior to the two excised spheres becomes the image of a single rectangular box. Let the spheres be denoted by $S_\pm$ and their radii by $\varrho_\pm$. We assume the centers of $S_\pm$ to be aligned along the x axis at a distance D from each other and introduce cylindrical coordinates (x, ρ, φ) about the x axis, i. e.

$$x = x, \qquad y = \rho\cos\varphi, \qquad z = \rho\sin\varphi, \tag{1}$$

with (x, y, z) being Cartesian coordinates. In the bispherical mapping the location of the $(x = 0)$ plane is chosen such that the product of the coordinates of inner and outer crossing points of the x axis with the surfaces $\partial S_\pm$ (see Fig. 1) is the same for both spheres. That is

$$x^{\mathrm{i}}_+ x^{\mathrm{o}}_+ = x^{\mathrm{i}}_- x^{\mathrm{o}}_- = a_0^2 \tag{2}$$

together with

$$x^{\mathrm{o}}_\pm - x^{\mathrm{i}}_\pm = \pm 2\varrho_\pm, \tag{3}$$

$$(x^{\mathrm{o}}_+ + x^{\mathrm{i}}_+) - (x^{\mathrm{o}}_- + x^{\mathrm{i}}_-) = 2D. \tag{4}$$

Here $a_0 > 0$ is the common distance of a ''geometric'' center of the two balls to the coordinate origin. It is given by

$$a_0 = \frac{1}{2} D^{-1}\sqrt{D^4 - 2D^2(\varrho_+^2 + \varrho_-^2) + (\varrho_+^2 - \varrho_-^2)^2}. \tag{5}$$

The bispherical coordinates (η, ξ, φ) are most easily introduced by the complex mapping

$$c = \mathrm{i}a_0 \coth\frac{\zeta}{2}, \tag{6}$$

where

$$c = \rho + \mathrm{i}x, \qquad \zeta = \eta + \mathrm{i}\xi \tag{7}$$

are complex combinations of cylindrical and bispherical coordinates, respectively. Explicitly, the coordinates ρ and x are given in terms of η and ξ as follows:

$$x = a_0 \frac{\sinh\eta}{\cosh\eta - \cos\xi} \tag{8}$$

$$\rho = a_0 \frac{\sin\xi}{\cosh\eta - \cos\xi}. \tag{9}$$

Note that the angle φ remains unchanged under this transformation.

A characteristic feature of the bispherical coordinates is that all coordinate lines

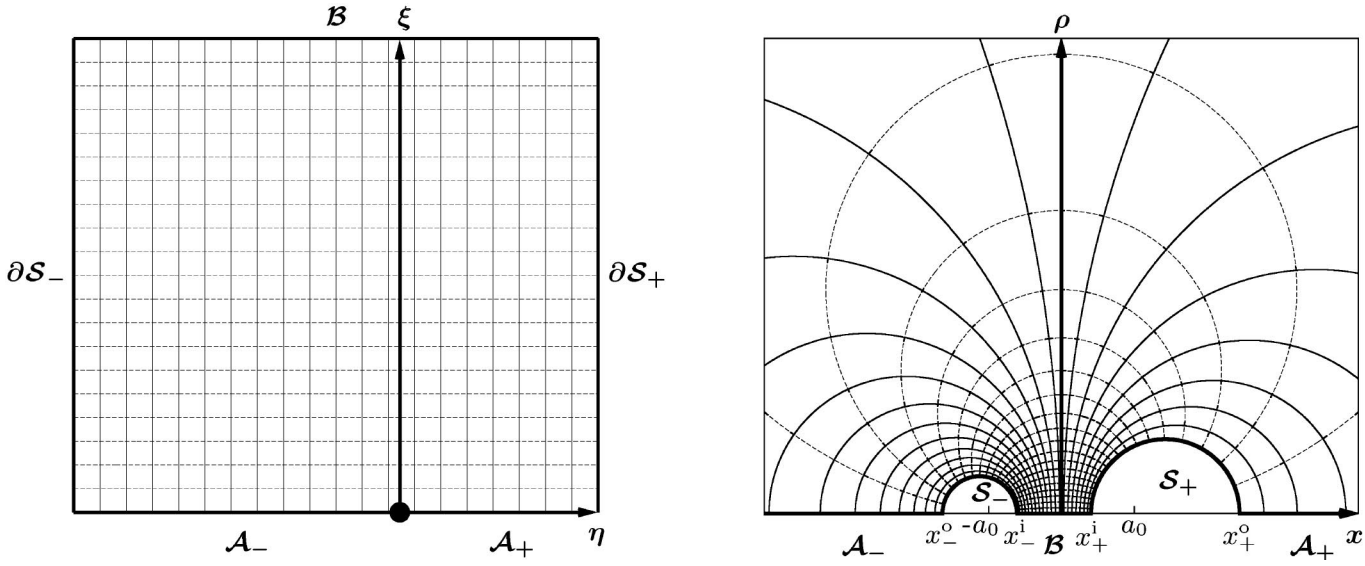

FIG. 1. Illustration of the bispherical mapping (6)–(9) for $D = 5\varrho_-$, $\varrho_+ = 2\varrho_-$ (with the azimuthal coordinate φ suppressed). The entire space exterior to the $S_\pm$ in the right panel is obtained as the image of the rectangular box displayed in the left panel. In both panels, solid and dashed curves correspond to constant η and ξ coordinate lines, respectively. The line (15) corresponding to spatial infinity is emphasized by a bullet.

$$\eta = \text{constant} \quad \text{and} \quad \xi = \text{constant} \tag{10}$$

correspond to circles in the cylindrical coordinates (x, ρ), see Fig. 1. In particular it follows that

$$(x - a_0 \coth\eta)^2 + \rho^2 = \frac{a_0^2}{\sinh^2\eta} \tag{11}$$

$$x^2 + (\rho - a_0 \cot\xi)^2 = \frac{a_0^2}{\sin^2\xi}. \tag{12}$$

Among these circles we find the surfaces $\partial S_\pm$ of the excised spheres, which are described by

$$\eta = \eta_\pm = \pm \operatorname{arsinh}\frac{a_0}{\varrho_\pm}. \tag{13}$$

From the preceding steps it becomes apparent that the entire space exterior to $S_\pm$ is obtained as the image of a single rectangular box,

$$\eta \in [\eta_-, \eta_+], \qquad \xi \in [0, \pi], \qquad \varphi \in [0, 2\pi). \tag{14}$$

While we have already seen that $\eta = \eta_\pm$ corresponds to the surfaces $\partial S_\pm$, the faces $\xi = 0$ and $\xi = \pi$ (in Fig. 1 denoted by $\mathcal{A}_\pm$ and $\mathcal{B}$) represent outer and inner sections of the x axis, respectively. Note that spatial infinity is obtained as the image of the line

$$\eta = 0 = \xi, \qquad \varphi \in [0, 2\pi). \tag{15}$$

At first glance, the bispherical mapping suggests a spectral expansion of the excision data in terms of the coordinates (η, ξ, φ). However, as will be demonstrated in Sec. III, the data are in general only C^0 at the above line corresponding to spatial infinity. We resolve this issue by another coordinate transformation, as will be discussed in Sec. IV.

III. BISPHERICAL SOLUTIONS OF THE LAPLACE EQUATION

We include this section about the bispherical solutions of the Laplace equation in order to illuminate some basic properties of the excision data, in particular, at spatial infinity. Exterior to $S_\pm$ consider

$$U_{xx} + U_{yy} + U_{zz} = 0 \tag{16}$$

subject to specific Dirichlet conditions that are enforced at the excision boundaries. In bispherical coordinates this reads as follows:

$$a_0^{-2}(\cosh\eta - \cos\xi)^{5/2}\Big(V_{\eta\eta} + V_{\xi\xi} + V_{\varphi\varphi}\csc^2\xi + V_\xi \cot\xi - \frac{1}{4}V\Big) = 0, \tag{17}$$

where the potential V is related to U via

$$U = V\sqrt{\cosh\eta - \cos\xi}. \tag{18}$$

In this formulation the solution can be found by separation of variables [34]. It reads

$$U = \sqrt{\cosh\eta - \cos\xi}\sum_{l=0}^{\infty}\sum_{m=-l}^{l}[\lambda_{lm}\mathrm{e}^{(l+1/2)\eta} + \mu_{lm}\mathrm{e}^{-(l+1/2)\eta}]Y_l^m(\xi, \varphi). \tag{19}$$

The coefficients λ_{lm} and μ_{lm} are obtained from an expansion of the known Dirichlet values of V at $\eta = \eta_\pm$ with respect to spherical harmonics Y_l^m.

We notice that the analytic behavior of the solution (19) at spatial infinity is determined by the factor

$$\sqrt{\cosh\eta - \cos\xi} = \sqrt{2\sinh\frac{\zeta}{2}\sinh\frac{\bar\zeta}{2}} = \frac{\sqrt{2}}{2}\sqrt{\eta^2 + \xi^2} + \mathcal{O}(|\zeta|^3), \tag{20}$$

which is only C^0 at $\zeta = 0$. Although one might argue that the decomposition (18) resolves this issue for the Laplace equation, this is not a strategy for solving general nonlinear elliptic equations since the corresponding solutions contain terms with and without the factor (20). We therefore pursue a different approach leading to new coordinates in which (20) is analytic.

IV. FOLDING INFINITY

The regularity problem addressed in the previous section is very closely related to issues discussed in [16], see formulas (48–50) therein. Indeed, introducing coordinates X and R via

$$Z = R + \mathrm{i}X = \sqrt{\zeta}, \tag{21}$$

where the square root is taken such that X and R are nonnegative in the computational domain (see Fig. 2), immediately yields that

$$\sqrt{\cosh\eta - \cos\xi} = \frac{\sqrt{2}}{2}(X^2 + R^2)\sqrt{\Big(1 + \sum_{k=1}^{\infty}\frac{Z^{4k}}{4^k(2k+1)!}\Big)\Big(1 + \sum_{k=1}^{\infty}\frac{\bar Z^{4k}}{4^k(2k+1)!}\Big)} \tag{22}$$

is analytic in X and R, in particular, at $X = R = 0$.

By performing the transformation (21) and leaving the azimuthal coordinate φ unchanged, the rectangular box (14) is folded about the line (15) such that a pentangular region is created upon which X and R are defined, see Fig. 2. Since for the spectral method the spectral coordinates (A, B, φ) introduced below are given on a cuboid, we draw a border that splits the pentangular region into two

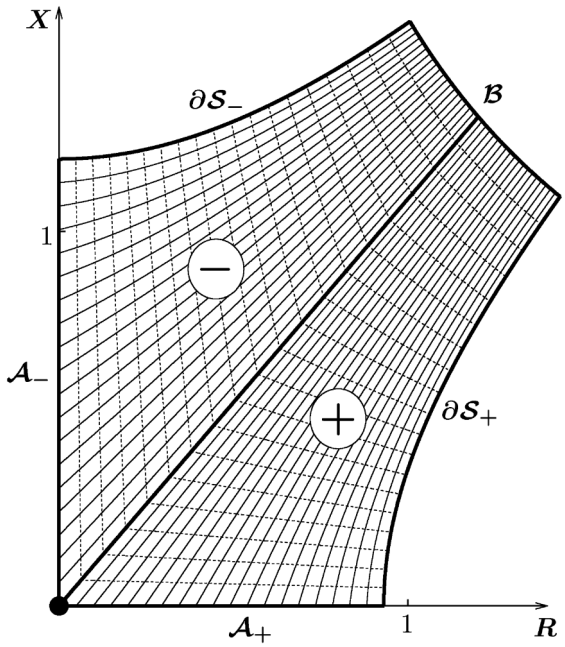

FIG. 2. Illustration of the mapping (21). The example displayed corresponds to the geometrical picture shown in Fig. 1. The border that separates the two quadrangular regions (±) is a line in this diagram. Solid and dashed curves correspond to constant A and B coordinate lines, respectively, (see (24)–(27)).

subdomains (±) of quadrangular shape. Now the coordinates (A, B) with

$$(A, B) \in [0, 1] \times [0, 1] \tag{23}$$

are mapped to values (X, R) on these subdomains via

(i) region +:

$$\begin{aligned} X &= -X^+AB + R_+A\sinh(\mu^+B) + X_0B\mathrm{e}^{\nu^+A}, \\ R &= -R^+AB + R_+A\cosh(\mu^+B) + R_0B\mathrm{e}^{-\nu^+A} \end{aligned} \tag{24}$$

(ii) region −:

$$\begin{aligned} X &= -X^-AB + X_-A\cosh(\mu^-B) + X_0B\mathrm{e}^{\nu^-A}, \\ R &= -R^-AB + X_-A\sinh(\mu^-B) + R_0B\mathrm{e}^{-\nu^-A} \end{aligned} \tag{25}$$

where

$$\begin{aligned} Z_\pm &= R_\pm + \mathrm{i}X_\pm = \sqrt{\eta_\pm}, \\ Z^\pm &= R^\pm + \mathrm{i}X^\pm = \sqrt{\eta_\pm + \mathrm{i}\pi}, \\ \mu^+ &= \operatorname{arsinh}(X^+/R_+), \\ \mu^- &= \operatorname{arsinh}(R^-/X_-), \\ \nu^\pm &= \ln(X^\pm/X_0). \end{aligned} \tag{26}$$

A value for X_0 ($R_0 = \pi/(2X_0)$) may be chosen in order to create subdomains of comparable size:

$$X_0 = \sqrt{X^-X^+}, \qquad R_0 = \sqrt{R^-R^+}. \tag{27}$$

With this transformation, the surfaces $\partial S_\pm$ are obtained for $A = 1$. Exterior and interior sections of the x axis (i.e. $\mathcal{A}_\pm$ and $\mathcal{B}$) are given by $B = 0$ and $B = 1$ respectively, and the common border between the two subdomains is described by $A = 0$.

V. THE NUMERICAL SCHEME

Our numerical scheme possesses a number of common features with the method described in [16] for the spectral calculation of puncture initial data. However, there are also specific differences, which we depict in the following paragraphs.

In a spectral approximation all functions U^κ to be determined by our elliptic boundary value problem are considered at specific gridpoints that correspond to the zeros or extrema of the spectral basis functions being used. Here we perform Chebyshev expansions with respect to A and B and a Fourier expansion with respect to φ. Since the quasistationary framework requires sophisticated boundary values at $\partial S_\pm$ for the initial data (see Sec. VI), we choose to use the extrema of the Chebyshev polynomials so as to have gridpoints lying on the boundary. That is, the gridpoints are given by

$$\begin{aligned} A_j &= \sin^2\!\left[\frac{\pi j}{2(n_A - 1)}\right], \qquad B_k = \sin^2\!\left[\frac{\pi k}{2(n_B - 1)}\right], \\ \varphi_l &= \frac{2\pi l}{n_\varphi} \end{aligned} \tag{28}$$

where

$$0 \le j < n_A, \qquad 0 \le k < n_B, \qquad 0 \le l < n_\varphi. \tag{29}$$

The numbers n_A, n_B and n_φ describe the spectral expansion orders of our scheme.

The next step in the scheme is the setting of a vector $\vec{U}$, whose components are derived from the values

$$U^{\kappa\pm}_{jkl} \tag{30}$$

of all functions U^κ at the above gridpoints (A_j, B_k, φ_l) in the two subdomains (±). The index $\kappa \in \{1, \ldots, \kappa_0\}$ labels the different functions appearing in the elliptic system, with κ_0 being the total number of equations ($\kappa_0 = 5$ for the quasistationary constraints discussed in Sec. VI).

A way to set $\vec{U}$ that works well in the context of the relaxation method described below is given by the following unique decomposition of U^κ:

$$U^\kappa(A, B, \varphi) = V^\kappa(A, B) + W^\kappa(A, B, \varphi), \tag{31}$$

$$W^\kappa(A, B, 0) = 0. \tag{32}$$

We use this decomposition and collect all values $V^{\kappa\pm}_{jk}$ and $W^{\kappa\pm}_{jkl}$ for $l > 0$ in order to build up the vector $\vec{U}$. This means that in our approach the $U^{\kappa\pm}_{jkl}$ are not stored directly in $\vec{U}$, but can be recovered from the entries of $\vec{U}$ through the above sum (31).

The collection of elliptic equations valid in the exterior of $S_\pm$, boundary conditions imposed at $A = 1$ (i.e. at $\partial S_\pm$), transition conditions to be imposed at $A = 0$ (i.e. at the common border) and specific regularity conditions that need to be fulfilled at $B = 0$ and $B = 1$ (i.e. at the x axis) yield a discrete nonlinear system

$$\vec{f}(\vec{U}) = 0 \tag{33}$$

of dimension

$$2\kappa_0 n_A n_B n_\varphi. \tag{34}$$

The corresponding solution describes the desired spectral approximation of the solution to our elliptic boundary value problem. Let us discuss in detail the several entries $f^{\kappa\pm}_{jkl}$ of the vectorial function $\vec{f}$:

(1) The spectral method enables us to calculate first and second derivatives of the U^κ from the values $U^{\kappa\pm}_{ijk}$ at the above grid points up to the chosen approximation order. Using them in the given elliptic equations evaluated at these grid points provides relations between the $U^{\kappa\pm}_{jkl}$. Note that the elliptic equations are only considered at inner grid points, i.e. for

$$1 \le j \le n_A - 2, \qquad 1 \le k \le n_B - 2, \qquad 0 \le l < n_\varphi, \tag{35}$$

thus filling

$$2\kappa_0 (n_A - 2)(n_B - 2) n_\varphi \tag{36}$$

entries of $\vec{f}$.

(2) In exactly the same manner, we use the boundary conditions valid at $A = 1$ to fill

$$2\kappa_0 n_B n_\varphi \tag{37}$$

entries of $\vec{f}$. Note that the boundary conditions are also considered at the x axis, i.e. at gridpoints with $j = 0$ or $j = n_B - 1$.

(3) Since the border between the two domains is some artificial transition surface that we have introduced, each function U^κ must be smooth there. In the formulation of the elliptic boundary value problem, this is ensured by requiring the U^κ to be continuous and to possess continuous normal derivatives at $A = 0$. These conditions are enforced along the entire border except the line (15) where the values of U^κ at infinity are imposed, thus leading altogether to

$$2\kappa_0 n_B n_\varphi \tag{38}$$

entries of $\vec{f}$.

(4) Special care is needed for setting the remaining discrete equations that correspond to regularity conditions along the x axis. Any function U that is smooth along the x axis with respect to Cartesian coordinates can be expanded in a Taylor series:

$$U(x, y, z) = U(x, 0, 0) + \rho[U_y(x, 0, 0)\cos\varphi + U_z(x, 0, 0)\sin\varphi] + \mathcal{O}(\rho^2) \tag{39}$$

from which it follows that

$$\lim_{\rho\to 0} U_{\varphi\varphi} = 0 \tag{40}$$

and

$$\lim_{\rho\to 0} (U_\rho + U_{\rho\varphi\varphi}) = 0. \tag{41}$$

The entire set of equations turns out to be solvable only if we consider both conditions (40) and (41). In particular, we require (40) at gridpoints with $\varphi > 0$ (i.e. $l > 0$) and (41) at gridpoints with $\varphi = 0$ (i.e. $l = 0$). The corresponding relations fill the remaining

$$4\kappa_0 (n_A - 2) n_\varphi \tag{42}$$

entries of $\vec{f}$. Note that different conditions need to be imposed if the underlying function U is not smooth along the x axis with respect to Cartesian coordinates. An example for this is given by the bispherical components of a vectorial function. In a subsequent publication we will discuss in detail this issue in connection with the momentum constraint equations.

In treating the system (33) we follow very much the approach described in [16], see section II therein. In particular, the solution is obtained by Newton-Raphson iterations, and the linear step inside this solver is performed with the preconditioned Biconjugate Gradient Stabilized (BCGSTAB) method [35]. In complete analogy to [16], we construct a second order finite difference representation of the Jacobian of (33), which will be used in the preconditioning step. Note that, because of the decomposition (31), for every gridpoint not only adjacent neighboring points need to be considered, but also the values for $l = 0$. The resulting finite difference Jacobian matrix has therefore at most $27\kappa_0$ nonvanishing entries per row.

A crucial difference to the method used in [16] is the performance of the preconditioning step in which an approximate solution of the system

$$J_{\mathrm{FD}} \delta\vec{U} = -\vec{f}(\vec{U}) \tag{43}$$

is obtained. The matrix J_{FD} appearing here represents the finite difference approximation of the Jacobian $J = \partial\vec{f}/\partial\vec{U}$ which was mentioned above. The vector $\delta\vec{U}$ describes a correction to $\vec{U}$ obtained through the values $\vec{f}(\vec{U})$.

We use a specific preconditioner that consists of successive plane relaxations with respect to the planes $\varphi =$ constant $= \varphi_l$. These plane relaxations in turn are composed of two different line relaxation schemes. We consider the method in more detail:

(1) For the first one of the two line relaxation schemes, let us pick one of the two regions ($\pm$) and some values j, l and κ. Then all values $\delta W^{\kappa\pm}_{jkl}$ (or $\delta V^{\kappa\pm}_{jk}$ for $l = 0$) along the coordinate line

$$A = A_j, B \in [0, 1], \varphi = \varphi_l \tag{44}$$

are determined simultaneously through (43) while all other entries of $\delta\vec{U}$ are held fixed. This gives a tridiagonal system of dimension n_B which can be solved with low computational cost.
We perform this procedure within the plane $\varphi = \varphi_l$ for all values j and κ and in both regions ($\pm$). Hereby, the loop over j takes on all even values first and then all odd ones, thus describing a ''zebra'' line relaxation scheme.

(2) Similarly, for the second line relaxation scheme k, l and κ are chosen, and all values $\delta W^{\kappa\pm}_{jkl}$ (or $\delta V^{\kappa\pm}_{jk}$ for $l = 0$) along the coordinate line

$$A \in [0, 1), B = B_k, \varphi = \varphi_l \tag{45}$$

are determined simultaneously through (43) in both regions ($\pm$), thus leading to a tridiagonal system of dimension $(2n_A - 3)$. Here we make use of the continuity of the U^κ at the transition border. Note that we leave out the values at the boundary $A = 1$, which for specific boundary conditions might be problematic for the convergence of the relaxation. We therefore obtain an update of these values only through the line relaxations described in 1.
Again we apply these steps within the plane $\varphi = \varphi_l$ for all values k and κ using a zebra loop with respect to k.

(3) The plane relaxation scheme within the plane $\varphi = \varphi_l$ is composed of several of the above orthogonal line relaxation schemes. A zebra loop with respect to l completes the relaxation method.

The preconditioning step, consisting of a number of such relaxations (a typical value is 20), is the fragile ingredient of the method. A simple reformulation of the boundary or regularity conditions might spoil the convergence of the scheme that otherwise is obtained through its iterative application. Since for interesting excision data the collection of elliptic equations and boundary conditions form a complicated system, it is very difficult to know how to pick a particular formulation in advance in order to ensure a stable convergent iteration. Nevertheless, for the relevant examples discussed in Sec. VI it was possible to cast the conditions into a suitable form.

Note that in general, relaxation schemes are computationally quite expensive if high resolution is used. In this case, it would be possible to include the relaxation scheme within a multigrid solver. However, since the spectral resolution can be chosen to be rather small (see Sec. VI), the method is already very efficient as it stands.

A preconditiong step consisting of 20 relaxation iterations gives a good approximation for the BCGSTAB method. Typically, only about 6 iterations within this scheme are needed to complete the linear Newton step. Thus the numerical scheme converges rapidly to the desired finite spectral approximation of the solution.

VI. QUASI-STATIONARY EXCISION DATA

The numerical scheme presented is applicable to an arbitrary set of elliptic equations that is valid in the exterior of two spheres and subject to specific boundary conditions required at the surfaces of these shells. In particular, it should prove fruitful for the calculation of a variety of initial data sets corresponding to binary black hole systems. In this section we apply the method to the important example, in which the initial data are given through the quasistationary framework.

In a first subsection we review the thin-sandwich approach which yields the set of elliptic equations to be considered. Next the isolated horizon boundary conditions describing a black hole in a quasiequilibrium state are discussed. The main focus of this section is on the presentation of exemplary solutions to the corresponding boundary value problem, which have been obtained by means of the scheme to an extremely high accuracy. In particular, we illustrate the strength of the method in the limiting case of very large ratios ϱ_+/ϱ_-.

A. The thin-sandwich equations

In the ADM-formulation of a '3 + 1'-splitting of the spacetime manifold, the general relativistic line element is written as

$$ds^2 = \gamma_{ij}(dx^i + \beta^i dt)(dx^j + \beta^j dt) - \alpha^2 dt^2, \tag{46}$$

where γ_{ij} is the 3-metric, and β^i and α are the shift vector and lapse function, respectively. Einstein's field equations can be split up into a set of constraint and evolution equations for the 12 quantities γ_{ij} and K_{ij} where

$$K_{ij} = \frac{1}{2\alpha}(\bar{\nabla}_i\beta_j + \bar{\nabla}_j\beta_i - \partial_t\gamma_{ij}) \tag{47}$$

is the extrinsic curvature ($\bar{\nabla}_j$ represents the spatial covariant derivative associated with γ_{ij}). The definition (47) yields one of two sets of six evolution equations.

In York's 'Conformal Thin-Sandwich Decomposition' [26] the evolution of the metric between two neighboring slices $t =$ constant is considered. More precisely, the Eqs. (47) make it possible to prescribe specific values for the initial time derivative of the conformal metric $\tilde{\gamma}_{ij}$, which is connected to γ_{ij} via $\gamma_{ij} = \psi^4\tilde{\gamma}_{ij}$ where ψ is a

''conformal factor''. Note that this splitting is unique only if we require some normalization for $\tilde{\gamma}_{ij}$, e.g. $\det(\tilde{\gamma}_{ij}) = 1$. In addition the extrinsic curvature is decomposed:

$$K^{ij} = \psi^{-10}\tilde{A}^{ij} + \frac{1}{3}\gamma^{ij}K, \qquad K = K^i_i. \tag{48}$$

In order to obtain initial data corresponding to a binary black hole in a quasistationary orbit, the constraint and evolution equations are considered in a comoving frame of reference in which the time derivatives of the metric quantities are assumed to be small initially. The thin-sandwich decomposition allows us to set

$$\partial_t \tilde{\gamma}_{ij} = 0 \tag{49}$$

in an initial slice $t = t_0$ from which by virtue of (47) it follows that

$$\tilde{A}_{ij} = \frac{\psi^6}{2\alpha}(\tilde{\mathbb{L}}\beta)_{ij} \tag{50}$$

with

$$(\tilde{\mathbb{L}}\beta)_{ij} = \tilde{\nabla}_i\beta_j + \tilde{\nabla}_j\beta_i - \frac{2}{3}\tilde{\gamma}_{ij}\tilde{\nabla}_k\beta^k. \tag{51}$$

In this formulation the constraint equations are given by

$$\tilde{\nabla}^2\psi - \frac{1}{8}\psi\tilde{R} - \frac{1}{12}\psi^5K^2 + \frac{1}{8}\psi^{-7}\tilde{A}_{ij}\tilde{A}^{ij} = 0 \tag{52}$$

$$\tilde{\nabla}_j(\tilde{\mathbb{L}}\beta)^{ij} - (\tilde{\mathbb{L}}\beta)^{ij}\tilde{\nabla}_j(\ln\alpha\psi^{-6}) - \frac{4}{3}\alpha\tilde{\nabla}^i K = 0. \tag{53}$$

Note that in these formulas $\tilde{\nabla}_j$ and $\tilde{R}$ are the spatial covariant derivative and the Ricci scalar, respectively, associated with the conformal metric $\tilde{\gamma}_{ij}$. Indices are raised and lowered with respect to this metric.

The Hamiltonian (52) and momentum constraints (53) are elliptic equations which can be used to determine the conformal factor ψ and the shift β^i respectively. Moreover, in the quasistationary framework it is possible to consider an additional equation which is obtained from the evolution equations through the requirement

$$\partial_t K = 0 \tag{54}$$

on the initial slice. This also gives an elliptic equation which determines the lapse function α:

$$\tilde{\nabla}^2(\alpha\psi) = \alpha\psi\left[\frac{1}{8}\tilde{R} + \frac{5}{12}\psi^5K^2 + \frac{7}{8}\psi^{-8}\tilde{A}_{ij}\tilde{A}^{ij}\right] + \psi^5\beta^i\tilde{\nabla}_i K. \tag{55}$$

Thus in total we have five elliptic Eqs. (52), (53), and (55) in order to determine the five quantities ψ, β^i and α. Note that the conformal metric $\tilde{\gamma}_{ij}$ and the trace K are free data that enter these equations. From the framework being presented no further restrictions on these quantities follow. In this paper we choose examples that correspond to maximal and conformally flat data, i.e. we set

$$K = 0 \tag{56}$$

and

$$\tilde{\gamma}_{ij} = \delta_{ij} \tag{57}$$

in the Cartesian coordinates (x, y, z) (with δ_{ij} denoting the Kronecker symbol).

B. Boundary conditions

The above quasistationary formulation is completed by a set of boundary conditions that control the data at the excision boundaries and at infinity. The excision boundary conditions are given through the ''Isolated Horizon Framework'' [10,25,29–32] (see also [3,4]) and describe black holes in a quasiequilibrium state. In particular the following is required:

(1) Within the initial slice, both excision boundaries are apparent horizons, i.e. two-dimensional hypersurfaces with S^2 topology and the property that the outgoing null vectors k possess vanishing expansion.
(2) Initially, the apparent horizon is tracked along k and its coordinate location does not move in the time evolution of the data.

Cook [10,25] incorporated these requirements into the thin-sandwich formulation and arrived at the following boundary conditions for ψ and β^i that are required at $\partial S_\pm$:

$$\tilde{s}^i\tilde{\nabla}_i(\ln\psi) = -\frac{1}{4}(\tilde{h}^{ij}\tilde{\nabla}_i\tilde{s}_j - \psi^2 J) \tag{58}$$

$$\beta^i = \alpha\psi^{-2}\tilde{s}^i + \beta^i_{||}. \tag{59}$$

Here the vector $\tilde{s}^i$ is the outward pointing unit vector normal to $\partial S_\pm$ (with respect to $\tilde{\gamma}_{ij}$) and $\tilde{h}_{ij} = \tilde{\gamma}_{ij} - \tilde{s}_i\tilde{s}_j$ the conformal metric induced on $\partial S_\pm$. The quantity J is given by

$$J = \psi^{-6}\tilde{h}_{ij}\tilde{A}^{ij} + \frac{2}{3}K \tag{60}$$

and the vector $\beta^i_{||}$ tangent to $\partial S_\pm$ is proportional to a conformal Killing vector of the conformal metric $\tilde{h}^{ij}$, with the proportional factor describing the angular velocity of the black hole. Note that the isolated horizon framework does not yield a boundary condition for the lapse α, which we are therefore free to choose.

In the examples discussed below we consider corotational black holes for which the angular velocity of the black holes, as seen within the comoving frame of reference, vanishes, i.e.

$$\beta^i_{||} = 0. \tag{61}$$

Moreover, we take the following boundary condition for the lapse, which was used among others in [10]:

$$\tilde{s}^i \tilde{\nabla}_i(\alpha\psi) = 0. \tag{62}$$

At infinity we impose the appropriate asymptotic behavior

$$\lim_{|\vec{r}|\to\infty} \psi = \lim_{|\vec{r}|\to\infty} \alpha = 1 \tag{63}$$

$$\lim_{|\vec{r}|\to\infty} [\beta^i - (\vec{\Omega} \times \vec{r})^i] = 0 \tag{64}$$

resulting from the fact that β^i is a shift vector in a comoving frame of reference that rotates with the angular velocity $\vec{\Omega}$. In the Cartesian coordinates $\vec{r} = (x, y, z)$ we take

$$\vec{\Omega} = \Omega \vec{e}_z \tag{65}$$

corresponding to an orbital motion of the black holes.

C. Examples

A well-known maximal and conformally flat solution to the above quasistationary boundary value problem is given by the Misner-Lindquist initial data [23,36] which are used for the evolution of a head-on collision of two black holes. These data are characterized by vanishing α and $\beta^i_{||}$ at the horizon (i.e. these data do not fulfill the condition (62) which we impose below) and moreover by $\Omega = 0$ (from which it naturally follows that they do not represent two orbiting black holes in a quasistationary state). In order to find quasistationary data, we need additional requirements such as the equality of ADM and Komar masses discussed below. Nevertheless, we start the investigation of the quasistationary boundary value problem in question by calculating solutions that represent modifications to the Misner-Lindquist data. In particular, we take the boundary condition (62) (instead of $\alpha = 0$) but retain all remaining conditions. Whereas the corresponding boundary value problem for a single black hole admits a solution which can be given explicitly [10,37], no exact solution is known in the binary case. However, we may take a superposition of the solutions known for the single black hole in order to create ''start up'' data for the Newton-Raphson scheme inside the numerical scheme. We consider the resulting solutions for $D = 10\varrho_-$ and four different choices of the radius ratio, $\varrho_+/\varrho_- \in \{1; 10; 100; 1000\}$. The excellent convergence of the spectral method has been checked globally for all functions U^κ appearing in our elliptic boundary value problem. We illustrate it in Fig. 3 for the total ADM mass of the system which is given in Cartesian coordinates by the following surface integral evaluated at infinity:

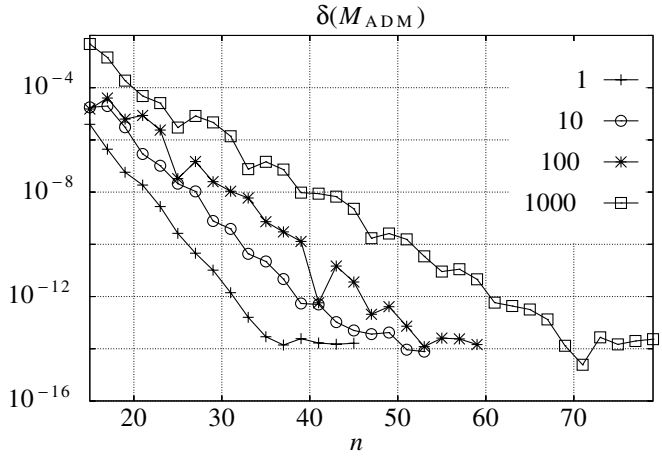

FIG. 3. The convergence of the ADM mass corresponding to binary black hole initial data sets with vanishing orbital angular velocity $\Omega = 0$. The geometrical parameters of the individual configurations are given by $D = 10\varrho_-$ and $\varrho_+/\varrho_- \in \{1; 10; 100; 1000\}$. For these axisymmetric calculations $n_A = n_B = n$ and $n_\varphi = 3$ have been chosen. We compared the corresponding results for the ADM masses to those of reference solutions with $n \in \{50; 60; 70; 80\}$ for the above choices of ϱ_+/ϱ_-.

$$M_{\mathrm{ADM}} = \frac{1}{16\pi} \int_\infty (\gamma_{ij,j} - \gamma_{jj,i}) d^2S_i. \tag{66}$$

We find that the convergence seems to be geometric, as exhibited by a roughly linear decrease of the error in this diagram.

Note that almost machine accuracy is reached for all ratios considered, thus proving that the method is well suited to the case of extreme radius ratios (and likewise to situations in which the distance D is extremely large). This may be clarified by the following considerations.

We know from the study of single black holes that the Dirichlet boundary values of the data remain restricted independent of the ratio ϱ_+/ϱ_-. However, because of the different scalings involved in the problem, one might not expect that the normal derivatives of the data at the surface of the small sphere remain bounded as ϱ_+/ϱ_- increases. This in turn would mean that a spectral expansion needs more and more resolution, which for extreme ratios becomes computationally unachievable.

To illustrate why nevertheless our method handles these critical cases with moderate computational effort, consider a special solution (19) to the Laplace equation (17), given by

$$V = \mathrm{e}^{(\eta_- - \eta)/2}. \tag{67}$$

It corresponds to the potential of a single point mass located at $(x, \rho) = (-a_0, 0)$ and possesses a finite value $V = 1$ at S_-. For the potential V we need not fold the rectangular box (14) at the line (15) in order to obtain

analyticity there, but may directly introduce spectral coordinates on (14), i.e. $(\hat{A}, \hat{B})$ via

$$\eta = \eta_- + (\eta_+ - \eta_-)\hat{A}, \qquad \xi = \pi\hat{B}. \tag{68}$$

Now the derivative

$$\frac{\partial V}{\partial \hat{A}}\bigg|_{\hat{A}=0} = -\frac{1}{2}(\eta_+ - \eta_-) \tag{69}$$

tends only logarithmically to infinity as $\varrho_-/a_0 \to 0$ (see (13)). Since the folding of (14) along (15) does not modify the qualitative behavior of the derivatives, a rapid spectral convergence emerges generally in these critical cases. Note that our coordinates are somewhat similar to those introduced in [38] via a logarithmic mapping in order to capture very different length scales appearing there.

In the second example we calculate initial data corresponding to two corotational black holes in a quasistationary orbit. It has been argued [3,4,10,25] that a suitable value for the angular velocity Ω is obtained by requiring the equality of the ADM mass and the Komar mass which is defined by the following surface integral at infinity:

$$M_{\mathrm{K}} = \frac{1}{4\pi}\int_\infty \gamma^{ij}(\bar{\nabla}_i\alpha - \beta^k K_{ik})d^2S_j. \tag{70}$$

In the example considered here, $D = 10\varrho_-$ and $\varrho_+ = \varrho_-$ have been chosen. For these data an orbital angular velocity $\Omega \approx 0.036\,975/\varrho_-$ emerges. Note that we introduce the vector

$$\hat{\beta}^i = \beta^i - (\vec{\Omega} \times \vec{r})^i \tag{71}$$

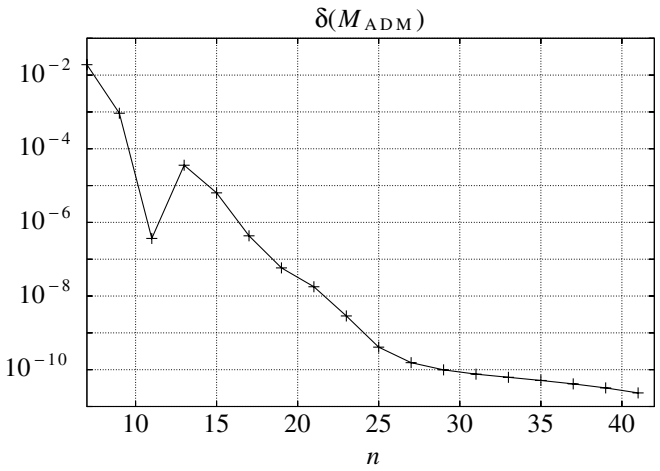

FIG. 4. The convergence of the ADM mass corresponding to a corotating binary black hole initial data set in a quasistationary orbit. The geometrical parameters of the configuration are given by $D = 10\varrho_-$ and $\varrho_+ = \varrho_-$. The data are characterized by the equality $M_{\mathrm{ADM}} = M_{\mathrm{K}}$ through which an orbital angular velocity of $\Omega \approx 0.036\,975/\varrho_-$ emerges. For these calculations the spectral resolutions $n_A = n_B = 2n_\varphi + 1 = n$ have been chosen. We compared the corresponding results for the ADM mass to that of the reference solution with $n = 51$.

into our numerical scheme which enables us to set definite values of the corresponding U^κ at infinity.

Again we illustrate the rapid convergence of the method by displaying the relative error of the total ADM mass, see Fig. (4). In contrast to the above axisymmetric examples, a roughly linear section of the curve for small resolution is followed by a much more flattened part as the accuracy approaches 10 digits.

A similar convergence rate was found for puncture initial data possessing individual linear momenta of the black holes [16]. In that paper the authors argue that an algebraic convergence of their scheme is caused by logarithmic terms in the expansion of the data at spatial infinity. From a specific numerical resolution on, this algebraic convergence rate governs the overall convergence. In the corresponding diagram (see figure 4 of [16]) this is exhibited by the fact that a roughly linear section of the curve for small resolution is followed by a more flattened part, which is exactly what we observe here. In a detailed mathematical study, we plan to clarify whether or not logarithmic terms also appear in the expansion of the above quasistationary data at spatial infinity, which would explain the behavior of the convergence rate in Fig. 4.

VII. CONCLUSIONS

In this paper we presented a numerical scheme that calculates binary black hole excision data by means of spectral methods. The central idea of the scheme is the introduction of specific coordinates that are related to bispherical coordinates, in order to permit rapid convergence of the spectral expansions. In particular, the entire space exterior to the two black holes is obtained as the image of two spatial domains within which the spectral expansions are carried out. A special formulation of the boundary and regularity conditions enables us to use a specific iterative technique to approach the solution that corresponds to the spectral approximation of the desired data.

The scheme has been used to calculate examples corresponding to the important quasistationary framework which is given by the conformal thin-sandwich decomposition together with the isolated horizon boundary conditions. It exhibits a rapid spectral convergence of the numerical solutions up to an extremely high accuracy. In particular, configurations with large radius ratios of the black holes may be considered up to this precision, with only moderate computational effort.

In future applications of the scheme we shall calculate a variety of initial data sets. The high accuracy of these data will enable us to investigate physical and mathematical properties thoroughly. Moreover, we intend to study several formulations of the constraint equations in order to select physically interesting data which correspond to a binary system with a realistic content of ingoing and outgoing radiation. For this it will prove fruitful to handle explicitly extreme configurations that correspond to limit-

ing cases (such as the test mass limit). Finally we plan to use the data in a dynamical evolution of the system which ultimately will help clear up the physical significance of the data being considered.

ACKNOWLEDGMENTS

The author wishes to thank B. Brügmann for many valuable discussions. Moreover he is grateful to D. Petroff for carefully reading the manuscript.

[1] S. Bonazzola, E. Gourgoulhon, and J.-A. Marck, Phys. Rev. D **58**, 104020 (1998).
[2] S. Bonazzola, E. Gourgoulhon, and J.-A. Marck, Phys. Rev. Lett. **82**, 892 (1999).
[3] P. Grandclément, E. Gourgoulhon, and S. Bonazzola, Phys. Rev. D **65**, 044021 (2002).
[4] E. Gourgoulhon, P. Grandclément, and S. Bonazzola, Phys. Rev. D **65**, 044020 (2002).
[5] M. Ansorg, A. Kleinwächter, and R. Meinel, Astron. Astrophys. **381**, L49 (2002).
[6] M. Ansorg, A. Kleinwächter, and R. Meinel, Astron. Astrophys. **405**, 711 (2003).
[7] M. Ansorg, A. Kleinwächter, and R. Meinel, Astrophys. J. **582**, L87 (2003).
[8] H. P. Pfeiffer, G. B. Cook, and S. A. Teukolsky, Phys. Rev. D **66**, 024047 (2002).
[9] H. P. Pfeiffer, L. E. Kidder, M. A. Scheel, and S. A. Teukolsky, Comput. Phys. Commun. **152**, 253 (2003).
[10] G. B. Cook and H. P. Pfeiffer, Phys. Rev. D **70**, 104016 (2004).
[11] S. Brandt and B. Brügmann, Phys. Rev. Lett. **78**, 3606 (1997).
[12] R. Beig and N. O'Murchadha, Classical Quantum Gravity **11**, 419 (1994).
[13] R. Beig and N. O'Murchadha, Classical Quantum Gravity **13**, 739 (1996).
[14] R. Beig, gr-qc/0005043.
[15] S. Dain, Phys. Rev. Lett. **87**, 121102 (2001).
[16] M. Ansorg, B. Brügmann, and W. Tichy, Phys. Rev. D **70**, 064011 (2004).
[17] J. Thornburg, Master's thesis, University of British Columbia, 1985.
[18] J. Thornburg, Classical Quantum Gravity **4**, 1119 (1987), http://stacks.iop.org/0264-9381/4/1119.
[19] G. B. Cook, M. W. Choptuik, M. R. Dubal, S. Klasky, R. A. Matzner, and S. R. Oliveira, Phys. Rev. D **47**, 1471 (1993).
[20] P. Diener, N. Jansen, A. Khokhlov, and I. Novikov, Classical Quantum Gravity **17**, 435 (2000).
[21] S. H. Hawley and R. A. Matzner, Classical Quantum Gravity **21**, 805 (2004).
[22] Hwei-Jang Yo, J. N. Cook, S. L. Shapiro, and T. W. Baumgarte, Phys. Rev. D **70**, 084033 (2004); Phys. Rev. D **70**, 089904(E) (2004).
[23] C. Misner, Phys. Rev. **118**, 1110 (1960).
[24] R. A. Matzner, M. F. Huq, and D. Shoemaker, Phys. Rev. D **59**, 024015 (1999).
[25] G. B. Cook, Phys. Rev. D **65**, 084003 (2002).
[26] J. W. York, Jr., Phys. Rev. Lett. **82**, 1350 (1999).
[27] H. P. Pfeiffer and J. W. York, Jr., Phys. Rev. D **67**, 044022 (2003).
[28] G. B. Cook, Living Rev. Relativity **3** 5 (2000), http://www.livingreviews.org/lrr-2000-5.
[29] A. Ashtekar, C. Beetle, O. Dreyer, S. Fairhurst, B. Krishnan, J. Lewandowski, and J. Wiśniewski, Phys. Rev. Lett. **85**, 3564 (2000).
[30] O. Dreyer, B. Krishnan, D. Shoemaker, and E. Schnetter, Phys. Rev. D **67**, 024018 (2003).
[31] A. Ashtekar and B. Krishnan, Phys. Rev. D **68**, 104030 (2003).
[32] J. L. Jaramillo, E. Gourgoulhon, and G. A. MenaMarugán, Phys. Rev. D **70**, 124036 (2004).
[33] G. Arfken, in *Mathematical Methods for Physicists* (Academic Press, Orlando, 1970), 2nd ed., p. 115.
[34] P. Moon and D. E. Spencer, in *Field Theory Handbook: Including Coordinate Systems, Differential Equations, and Their Solutions* (Springer-Verlag, New York, 1988), 2nd ed., p. 110.
[35] R. Barrett, M. Berry, T. Chan, J. Dongarra, V. Eijkhout, C. Romine, and H. van der Vorst, Templates for the Solution of Linear Systems: Building Blocks for Iterative Methods, http://www.netlib.org/templates/.
[36] R. W. Lindquist, J. Math. Phys. (N.Y.) **4**, 938 (1963).
[37] F. Estabrook, H. Wahlquist, S. Christensen, B. DeWitt, L. Smarr, and E. Tsiang, Phys. Rev. D **7**, 2814 (1973).
[38] M. Ansorg and D. Petroff, Phys. Rev. D **72**, 024019 (2005).